Article

Design of an omnidirectional camouflage device with anisotropic confocal elliptic geometry in thermal-electric field

Huolei Feng,
Xingwei Zhang,
Yuekai Zhang,
Limin Zhou,
Yushan Ni

niyushan@fudan.edu.cn

Highlights

Omnidirectional
camouflage device with
anisotropic geometry is
constructed

Anisotropic matrix
dominates the thermal-
electric camouflage effect
omnidirectionally

A multilayered composite
structure contributes to
the experimental
implementation

Article

Design of an omnidirectional camouflage device with anisotropic confocal elliptic geometry in thermal-electric field

Huolei Feng,[1] Xingwei Zhang,[2] Yuekai Zhang,[2] Limin Zhou,[1] and Yushan Ni[1,3,*]

SUMMARY

The designed confocal elliptical core-shell structure can realize the omnidirectional camouflage effect without disturbing temperature and electric potential profiles as the directions of heat flux and electric current change. Based on the anisotropy of the confocal ellipse, the anisotropic effective parameters of the confocal elliptical core-shell structure are derived under different heat flux and electric current launching. Then, the matrix material should be anisotropic as the effective parameters to satisfy the omnidirectional camouflage effect, which is demonstrated numerically. In addition, we present a composite structure to realize the anisotropic matrix. The experimental results show that the camouflage device embedded in the composite structure can eliminate the scattering caused by the elliptical core under different directions of heat flux and electric current, thus achieving the omnidirectional thermal-electric camouflage effect experimentally. The omnidirectional camouflage effect in thermal and electric fields can greatly widen the application fields of this device with anisotropic geometry.

INTRODUCTION

Since the advent of transformation optics (Pendry et al., 2006) and neutral inclusion (Zhou and Hu, 2006; He and Wu, 2013), metamaterials have been in the promising field, which have been successfully demonstrated in various communities, such as optics (Pendry et al., 2006), electromagnetic waves (Schurig et al., 2006; Chen and Chan, 2007; Rahm et al., 2008; Han and Zhang, 2020; Berry and Rumpf, 2020; Fakheri et al., 2020; Asrafali et al., 2021), acoustics (Zhang et al., 2011; Popa et al., 2011), elastic mechanics (Brun et al., 2009; Farhat et al., 2009), direct current (DC) electric fields (Yang et al., 2012; Jiang et al., 2012; Han et al., 2014a; 2019; Feng and Ni, 2022a, 2022b), and thermotics (Fan et al., 2008; Narayana and Sato, 2012; Guenneau et al., 2012; Narayana et al., 2013; Han et al., 2014b, 2018; Li et al., 2015; 2018, 2019, 2020, 2021, 2022; Yang et al., 2017, 2021; Xu et al., 2020a; Feng and Ni, 2022a, 2022b). These metamaterials exhibit excellent performances in their certain conditions. With the further development of research, the requirements of advanced and multiphysical metamaterials are much more desirable for practical applications compared with previous metamaterials, which only work in a single physical field. Thermal-electric metamaterials, which can control both temperature and electric fields, have attracted extensive research interest. The thermal-electric metamaterial possessing both thermal and electrical cloaking functionality was theoretically explored (Li et al., 2010). The thermal-electric cloaking effect using a porous metamaterial structure was further experimentally demonstrated (Ma et al., 2014). A temperature-dependent transformation method was established to realize different thermal-electric functions in temperature-dependent backgrounds (Lei et al., 2021). Three representative devices with bilayer schemes for manipulating coupled thermal-electric transport were also constructed (Qu et al., 2021). Recently, some researchers have been devoted to study the metamaterials capable of satisfying the camouflage effect in thermal-electric fields simultaneously using the method of neutral inclusion. Here, the thermal-electric camouflage device refers to a device that can eliminate the scattering caused by any objects, thus making these objects invisible in thermal and electric fields simultaneously, just as nothing exists along the paths. The camouflage property can protect the objects and confuse the detector, which can be employed to design the illusion object possessing the same signatures as the target object to be protected, especially in the aerospace field. Simultaneously, the camouflage effect can also be used to construct the invisible sensors, which can sense and camouflage in multiphysical fields. The core coated by a monolayer shell was constructed, which can camouflage in thermal-electric fields simultaneously to a certain extent

[1]Department of Aeronautics and Astronautics, Fudan University, Shanghai 200433, China

[2]Key Laboratory of Advanced Ship Materials and Mechanics, College of Aerospace and Civil Engineering, Harbin Engineering University, Harbin 150001, China

[3]Lead contact

*Correspondence: niyushan@fudan.edu.cn

https://doi.org/10.1016/j.isci.2022.104183

(Yang et al., 2015). The core coated by a bilayer shell was further designed, which can camouflage in thermal-electric field accurately (Zhang et al., 2021). References (Yang et al., 2015; Zhang et al., 2021) reveal the circular thermal-electric camouflage effects from different perspectives, and the isotropic circular geometry leads to the isotropy of the matrix material for realizing the camouflage effect. However, according to the practical application fields, the geometry of the camouflage device may not be limited to circles, and the anisotropic geometries of confocal ellipse, diamond shape, rectangle, etc. have been employed in other functional devices in specific environments. To expand the application fields of the camouflage device, some researchers started analyzing the thermal-electric camouflage effect with anisotropic geometry. The ellipsoidal bifunctional thermal-electric camouflage device was designed, and the camouflage effect was also analyzed (Zhang et al., 2020). Unfortunately, reference (Zhang et al., 2020) ignored the anisotropy of matrix material caused by the anisotropic confocal ellipse, which leads to the disturbances of isothermal lines and equipotential lines in the matrix under different directions of heat flux and electric current.

To eliminate the disturbances of temperature and electric potential fields caused by the geometric anisotropy of the camouflage device omnidirectionally, the confocal elliptical core-shell structure based on the anisotropic matrix is designed, inspired by the construction of omnidirectional thermal metadevices (Han et al., 2018). The proposed confocal elliptical core-shell structure is suitable for different directions of heat flux and electric current, which can achieve the omnidirectional camouflage effect of the elliptical core region in thermal and electric fields. In this paper, the elliptical core region represents the camouflage region, and the elliptical shell region is denoted as the camouflage device. We derive the anisotropic effective parameters of confocal elliptical core-shell structure under different heat flux and electric current launching, which coincide with the matrix material parameters. Then, we numerically demonstrate the omnidirectional thermal-electric camouflage effect by applying the anisotropic matrix material described earlier. In addition, we construct a composite structure based on the effective medium theory and single-particle structure method to realize the anisotropic matrix, and the experiments are carried out to demonstrate the omnidirectional camouflage effect based on the composite structure in thermal and electric fields. The quantitative comparisons are also employed to make the experimental results much more convincing.

RESULTS AND DISCUSSION

The omnidirectional camouflage effect with anisotropic matrix material

To eliminate the disturbances of thermal and electric fields caused by the confocal elliptical core structure when the directions of heat flux and electric current are unknown, the thermal and electric conductivities of matrix material should coincide with the effective parameters of the core-shell structure. The detailed derivations of anisotropic effective material parameters of confocal elliptical core-shell structure are presented in STAR Methods. As for the realization of the omnidirectional camouflage effect of the core region, we need to define the material and geometric parameters of the core and shell to obtain the anisotropic matrix material. Firstly, the materials of the core and shell are arbitrary. Here, we select air and 6061 aluminum as the materials of core and shell. The material parameters of the core and shell are $\kappa_1 = 0$ W/(m*K), $\kappa_2 = 155$ W/(m*K) for the thermal conductivity and $\sigma_1 = 0$ S/m, $\sigma_2 = 2.49E7$ S/m for the electric conductivity, respectively (Zhang et al., 2020). Secondly, the geometric parameters of the core and shell are given as $lc_1 = 3$cm, $lc_2 = 2$cm and $ls_1 = 4.72$cm, $ls_2 = 4.16$cm, respectively based on the confocal characteristics of elliptical core-shell structure and the geometric parameter optimization. Finally, the anisotropic effective thermal and electrical conductivities of the matrix could be calculated under different heat flux or electric current directions based on the Equations 9 and 10 to design the omnidirectional confocal elliptical camouflage device in thermal and electric fields.

The finite element numerical simulations have been conducted to demonstrate the omnidirectional camouflage effect of the elliptical air core under different directions of heat flux and electric current ($\varphi = 0°$, $45°$ and $90°$) according to the material and geometric parameters described earlier. The temperature boundary conditions of the computational domain are set to 293.15 and 273.15K, and the other sides are set to insulation boundary conditions. The simulation results of temperature profiles are shown in Figure 1, in which the field distributions are normalized by the maximum and minimum values. For comparison, we simulate three different models. Figures 1A, 1B, and 1C represent the normalized temperature fields of models with anisotropic matrix material, air core without confocal elliptical camouflage device, and air core with confocal elliptical camouflage device, respectively under the horizontal ($\varphi = 0°$) heat flux launching. For the oblique heat flux launching ($\varphi = 45°$) (or vertical heat flux launching ($\varphi = 90°$)), Figures 1D, 1E, and 1F
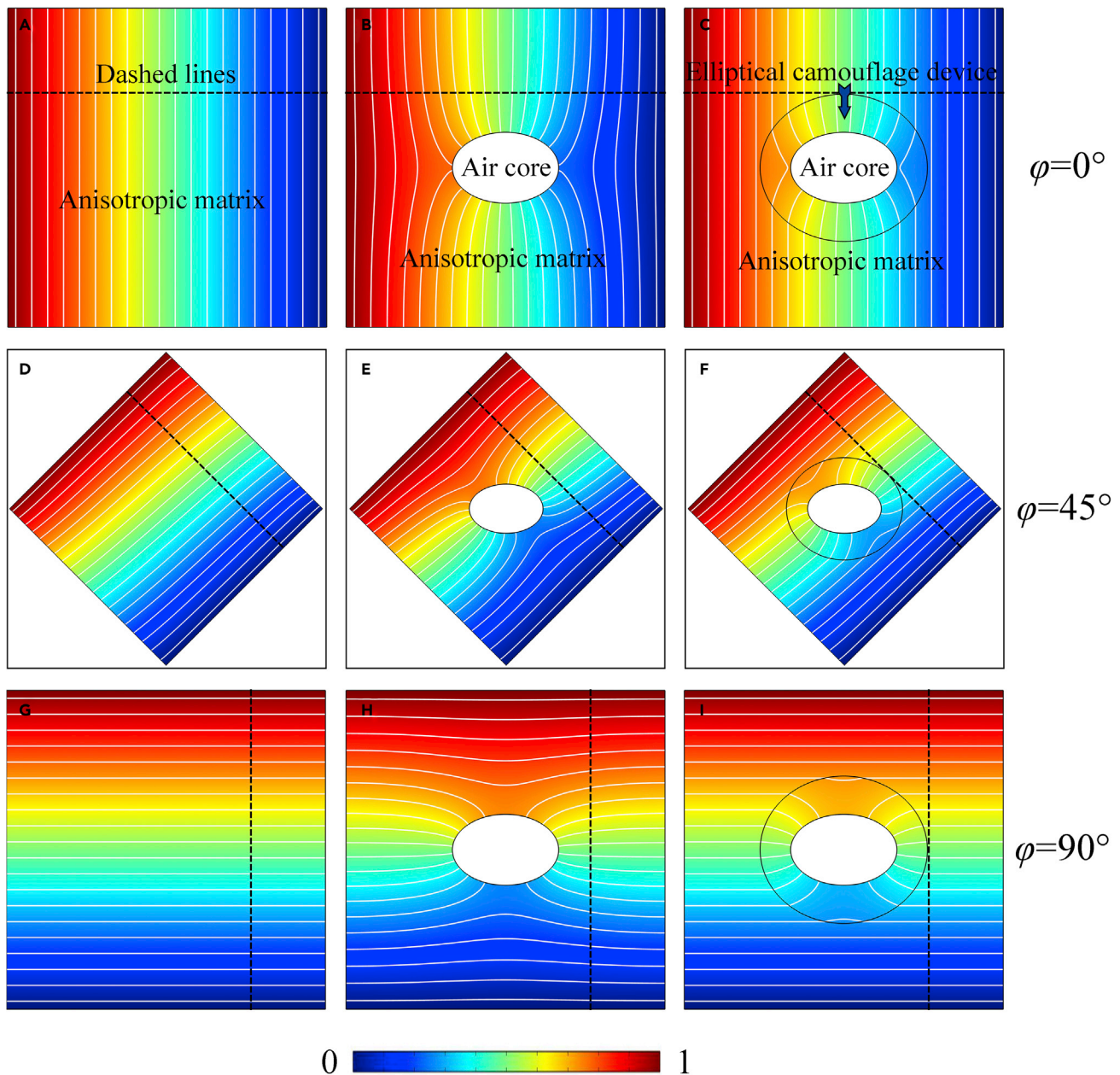
Figure 1. Normalized temperature distributions with different directions of heat flux

(A, D, and G) The normalized temperature distributions of model with anisotropic matrix.

(B, E, and H) The normalized temperature distributions of model with a pure air core embedded in the anisotropic matrix.

(C, F, and I) The normalized temperature distributions of model with an air core coated by the elliptical camouflage device. The white solid lines represent the isothermal lines.

(or Figures 1G, 1H, and 1I) represent the normalized temperature fields of the same models corresponding to Figures 1A, 1B, and 1C, respectively.

Compared with the normalized temperature fields of the models with anisotropic matrix material illustrated in Figures 1A, 1D, and 1G, it can be obviously found that the air core embedded into the matrix will cause the disturbances of isothermal lines with different directions of heat flux because of the different thermal conductivities of air core and matrix, as shown in Figures 1B, 1E, and 1H. Then, the disturbances of isothermal lines will be eliminated under the work of the confocal elliptical camouflage device, and the
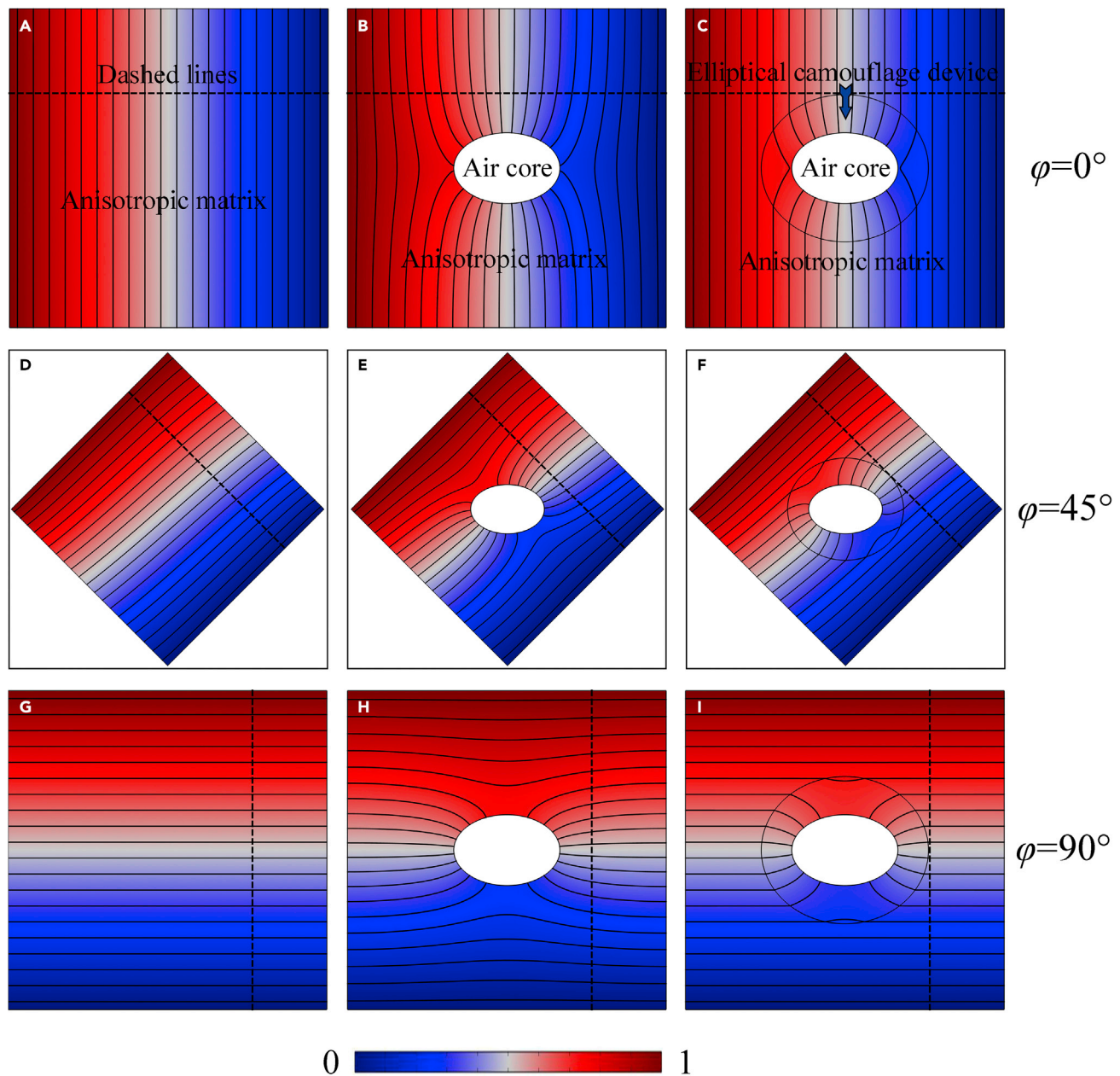
Figure 2. Normalized electric distributions with different directions of electric current

(A, D, and G) The normalized electric distributions of model with anisotropic matrix.

(B, E, and H) The normalized electric distributions of model with a pure air core embedded in the anisotropic matrix.

(C, F, and I) The normalized electric distributions of model with an air core coated by the elliptical camouflage device. The black solid lines represent the equipotential lines.

isothermal lines in the matrix become straight again, as shown in Figures 1C, 1F, and 1I. It means that no matter the directions of heat flux are 0°, 45°, and 90°, the camouflage device embedded in the anisotropic matrix material can eliminate the disturbances of isothermal lines caused by the elliptical air core, thus achieving the omnidirectional thermal camouflage effect of the core.

The prior analyses mainly focus on the normalized temperature fields. As for the electric fields, the camouflage device still works with different directions of electric current. Here, we define the electric boundary conditions as 5 and 0V, and the other sides still remain insulated. The electric distributions normalized by
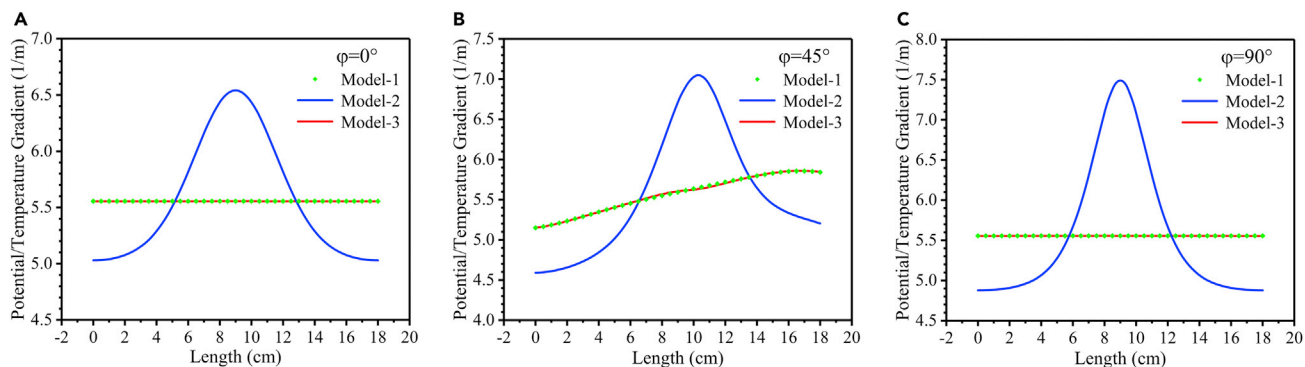
Figure 3. The normalized electric potential or temperature gradients along the dashed lines

(A) The normalized gradients under the horizontal ($\varphi = 0°$) heat flux and electric current launching.

(B) The normalized gradients under the oblique ($\varphi = 45°$) heat flux and electric current launching.

(C) The normalized gradients under the vertical ($\varphi = 90°$) heat flux and electric current launching. Model-1, Model-2 and Model-3 represent the models with anisotropic matrix material, the air core without confocal elliptical camouflage device, and the air core with confocal elliptical camouflage device, respectively.

the maximum and minimum values are presented in Figure 2 numerically, in which the first row (Figures 2A, 2B, and 2C), the second row (Figures 2D, 2E, and 2F), and the third row (Figures 2G, 2H, and 2I) correspond to the horizontal ($\varphi = 0°$), oblique ($\varphi = 45°$), and vertical ($\varphi = 90°$) electric current launching, respectively, and the first column (Figures 2A, 2D, and 2G), the second column (Figures 2B, 2E, and 2H), and the third column (Figures 2C, 2F, and 2I) represent the normalized electric fields of models with anisotropic matrix material, air core without confocal elliptical camouflage device, and air core with confocal elliptical camouflage device, respectively. Similar to the results of temperature distributions, the disturbances of equipotential lines in the Figures 2B, 2E, and 2H with different directions of electric current have been eliminated in the Figures 2C, 2F, and 2I under the work of the camouflage device, and the electric distributions of matrix in the Figures 2C, 2F, and 2I coincide with those in the Figures 2A, 2D, and 2G, thus realizing the omnidirectional electric camouflage effect. Based on the prior analyses, we have numerically demonstrated the theory of the anisotropic effective parameters presented in STAR Methods, indicating that the confocal elliptical camouflage device embedded in the anisotropic matrix material can omnidirectionally eliminate the scatterings caused by the elliptical air core in thermal and electric fields perfectly.

Further, we quantitatively analyze the omnidirectional camouflage effect. For quantitative comparison, we export the temperature gradient and electric potential gradient on the dashed lines in Figures 1 and 2.
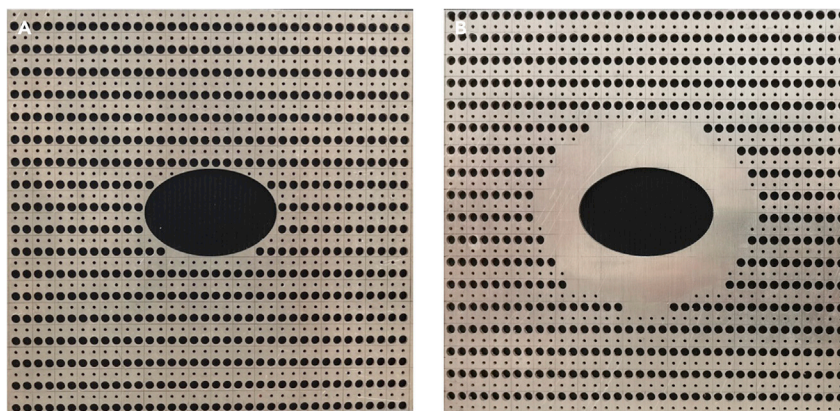
Figure 4. The experimental samples whose sizes are 18 × 18 cm with a thickness of 2 mm

(A) The reference experimental sample with only the air core in the composite structure of the matrix.

(B) The functional experimental sample with the camouflage device wrapped around the air core in the composite structure of the matrix.
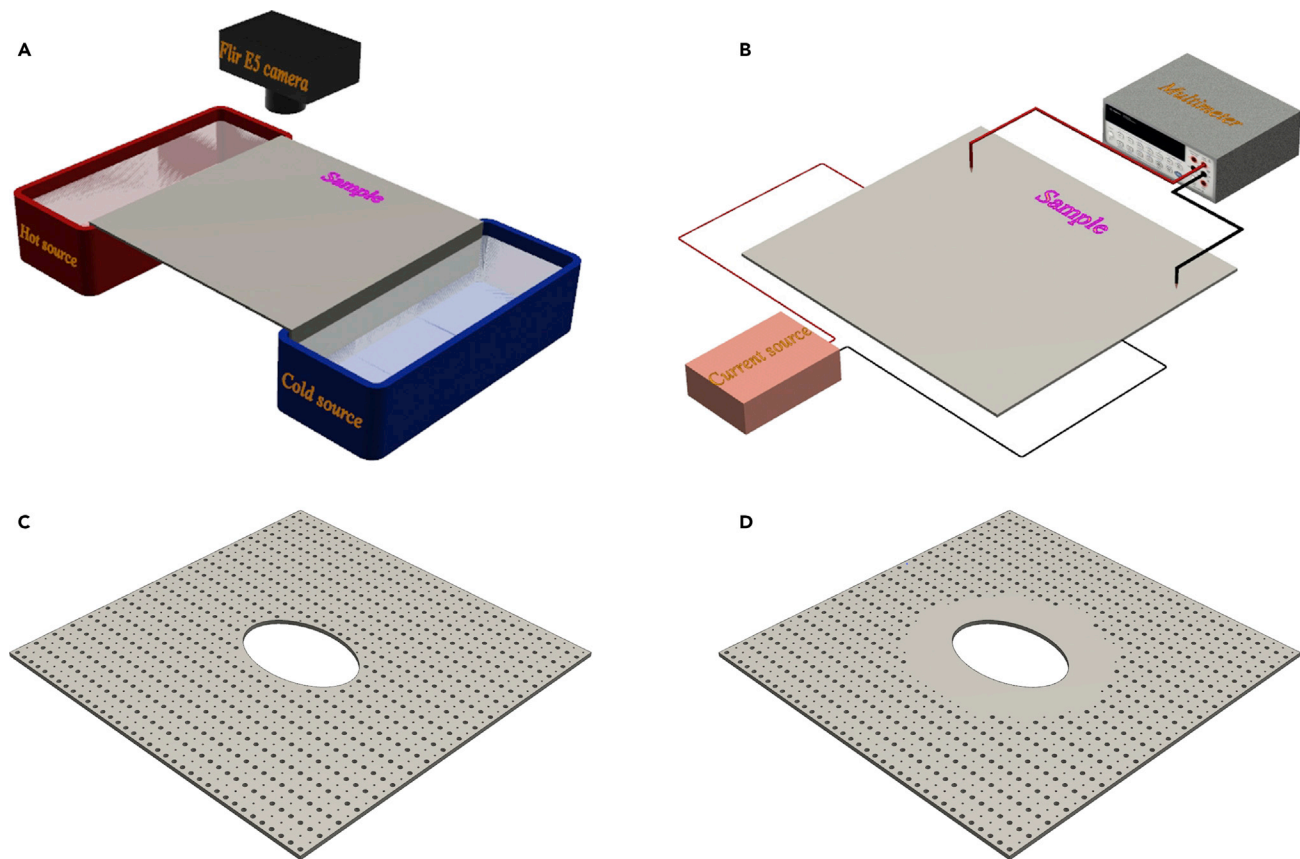
Figure 5. The diagrams of experimental setups
(A) Thermal experimental setup.
(B) Electric experimental setup.
(C) The reference experimental sample.
(D) The functional experimental sample.

Because the temperature and electric distributions have been normalized by the maximum and minimum values, the temperature gradients along the dashed lines coincide with the electric potential gradients. The results corresponding to horizontal ($\varphi = 0°$), oblique ($\varphi = 45°$), and vertical ($\varphi = 90°$) directions of heat flux and electric current are presented in Figures 3A, 3B, and 3C, respectively.

It could be seen from Figure 3 that the electric potential or temperature gradients of Model-1 and Model-3 are consistent on the dashed lines under different directions of heat flux and electric current. However, the electric potential or temperature gradient of Model-2 in the matrix is a value that changes with length, which varies from 5.03 (1/m) to 6.54 (1/m) for $\varphi = 0°$, from 4.59 (1/m) to 7.04 (1/m) for $\varphi = 45°$, and from 4.88 (1/m) to 7.49 (1/m) for $\varphi = 90°$. It means that owing to the function of confocal elliptical camouflage device, the disturbances of temperature and electric potential fields caused by the elliptical air core are eliminated, and the completely different electric potential or temperature gradient of Model-2 will tend to the values presented in Model-1 and Model-3. Through the earlier discussions, we have numerically demonstrated the feasibility of the anisotropic matrix material, which is capable of realizing the omnidirectional thermal-electric camouflage effect of the elliptical air core.

Experimental demonstration of the omnidirectional camouflage effect

In the previous section, the anisotropic matrix is used to design the omnidirectional confocal elliptical camouflage device. However, the anisotropic matrix also limits the practical experimental implementation. To overcome the limitation of the anisotropic matrix and keep the camouflage effect, we further design a composite structure with natural materials (Figure S2C) to realize the anisotropic matrix. The
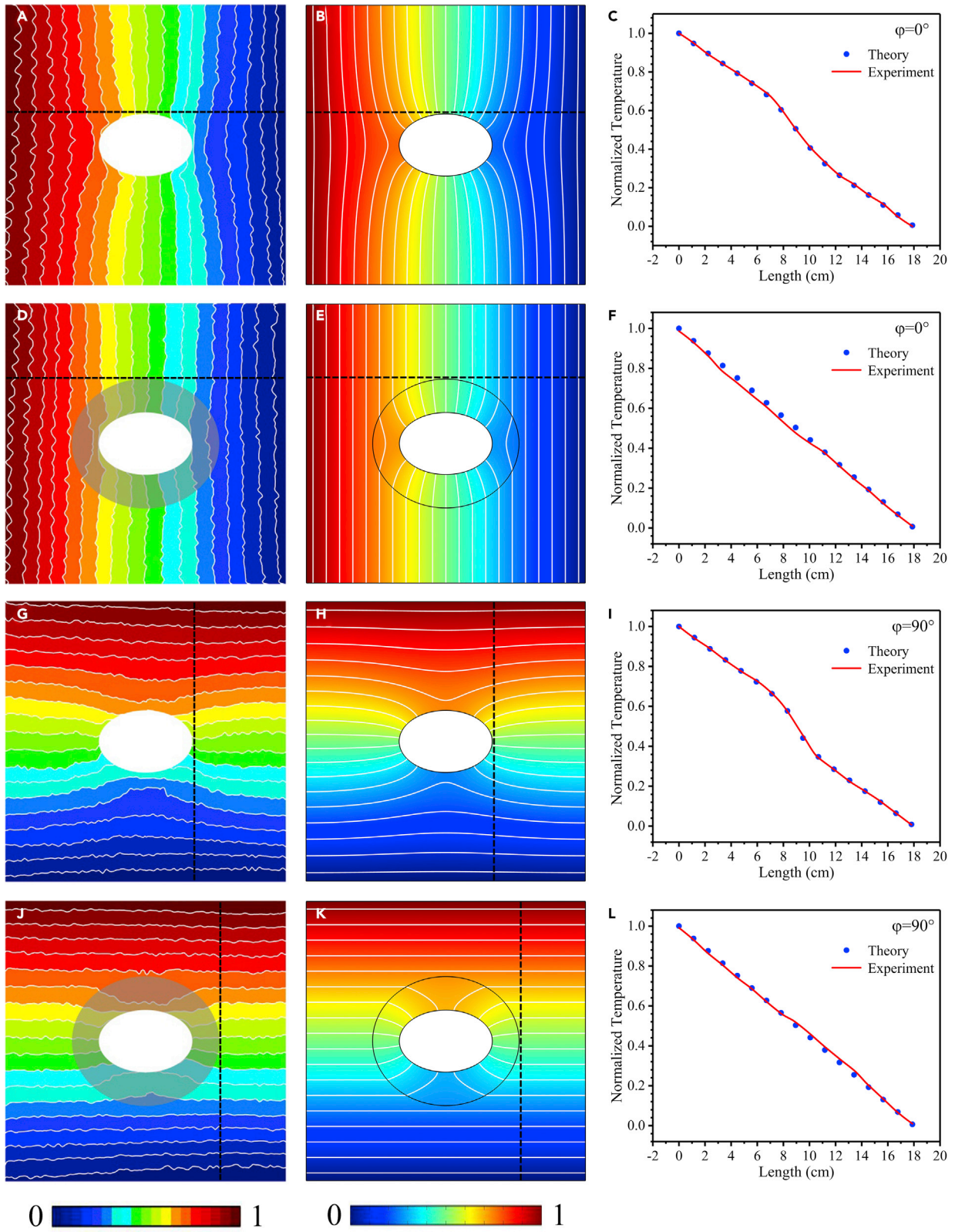
Figure 6. Normalized temperature distributions

(A and D) The experimental measurements of thermal fields under the horizontal heat flux launching.

(G and J) The experimental measurements of thermal fields under the vertical heat flux launching.

(B and E) The theoretical predictions of thermal fields under the horizontal heat flux launching.

(H and K) The theoretical predictions of thermal fields under the vertical heat flux launching.

(C, F, I, and L) The quantitative comparisons between the experimental measurements and theoretical predictions corresponding to different directions of heat flux.

detailed processing approaches are shown in STAR Methods. Then, based on the composite structure of the matrix, the experiments are carried out to demonstrate the omnidirectional camouflage effect of the elliptical air core. Here, considering the operability and flexibility of the experimental setups and data collections, we mainly discuss the conditions with horizontal and vertical directions of heat flux and electric current.

Experimental samples

We fabricate two experimental samples by utilizing laser cutting of a 6061 aluminum plate. The core region is carved with an air ellipse with a major (or minor) semiaxis of 3 cm (or 2 cm) embedded in the middle of the 6061 aluminum plate. The shell region (camouflage device) is still 6061 aluminum with a major (or minor) semiaxis of 4.72 cm (or 4.16 cm) wrapped around the core. The matrix composed of 6061 aluminum and air circular holes is an alternating-multilayered structure with 36 layers, each of which is 0.5 cm thick. The radii of the air circular holes in the background are 0.075 and 0.2 cm for the alternating layers, respectively. Figure 4A (Figure 4B) represents the experimental sample that the air core without (with) camouflage device is embedded in the composite structure of the matrix.

Experimental setups

The diagrams of thermal and electric experimental setups are shown in Figure 5. In the thermal experimental setup, temperature on one side of the sample is achieved by a heating device, whereas the other side is connected to the mixture of ice and water. Simultaneously, the insulated plastic films are deposited on the surface of each sample to eliminate the high reflection by 6061 aluminum and thermal convection by air. We use the Flir E5 infrared camera to obtain the temperature profiles of the samples. As for the electric experiment, a powerful DC current source device is used to provide a large electric current passing through the samples. Simultaneously, the 34401A digital multimeter is employed to detect the electric profiles of the samples. To demonstrate the omnidirectional camouflage effect of the air core, we conduct two experiments corresponding to the horizontal ($\varphi = 0°$) and vertical ($\varphi = 90°$) directions of heat flux and electric current, respectively.

Experimental results

Figures 6A and 6D represent the experimental-normalized temperature fields of the experimental samples corresponding to Figures 4A and 4B, respectively, under the horizontal heat flux launching ($\varphi = 0°$). For the vertical heat flux launching ($\varphi = 90°$), Figures 6G and 6J represent the experimental-normalized temperature fields of the same models corresponding to Figures 6A and 6D, respectively. It is clearly seen that when the heat flux is along the horizontal direction, the air core without confocal elliptical camouflage device could distort isothermal lines in the matrix (Figure 6A), thus making itself visible by the thermal detector. When the air core is coated by the confocal elliptical camouflage device, the isothermal lines return to be uniform (Figure 6D), which makes the air core camouflage in the matrix to be perfect. As the heat flux is along the vertical direction, the disturbances of temperature field caused by the elliptical air core (Figure 6G) are still eliminated under the function of a confocal elliptical camouflage device (Figure 6J). To make the experimental results more convincing, we further perform the finite element numerical simulations using the theoretically derived material parameters. The geometric parameters of the simulation models are consistent with the experiments. Figures 6B and 6E represent the normalized simulation results with $\varphi = 0°$ corresponding to the experimental results Figures 6A and 6D, respectively. Similarly, Figures 6H and 6K represent the normalized simulation results with $\varphi = 90°$ corresponding to experimental results Figures 6G and 6J, respectively. Obviously, the isothermal lines are disturbed and bend to the elliptical air core under horizontal heat flux (Figure 6B) or vertical heat flux (Figure 6H) launching, and the disturbances will be eliminated when the confocal elliptical camouflage device is applied around the air core illustrated in Figures 6E or 6K. For quantitative comparison, we export the normalized temperature on the dashed lines in Figure 6. Figures 6C and 6F (or Figures 6I
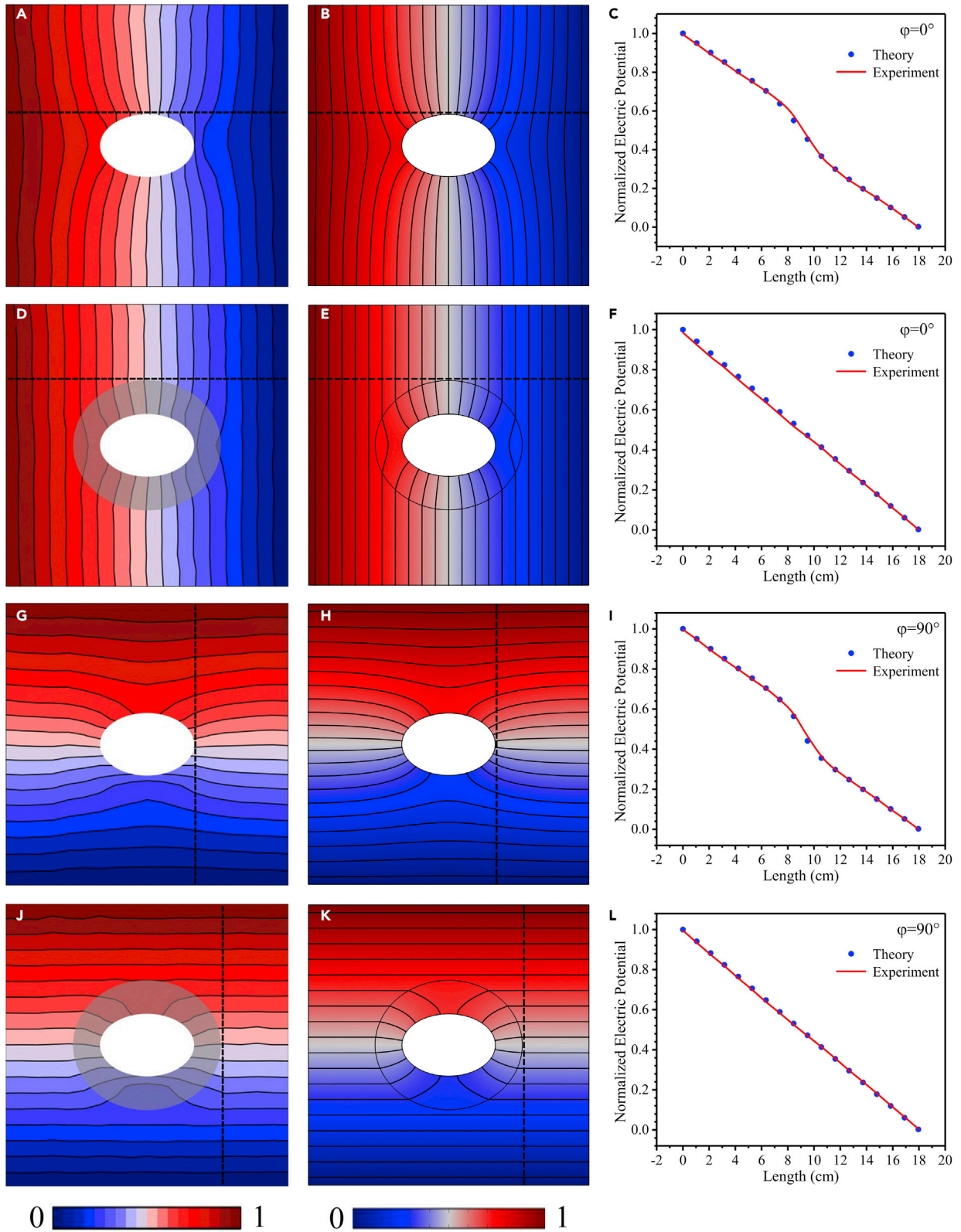
Figure 7. Normalized electric distributions

(A and D) The experimental measurements of electric fields under the horizontal electric current launching.

(G and J) The experimental measurements of electric fields under the vertical electric current launching.

(B and E) The theoretical predictions of electric fields under the horizontal electric current launching.

(H and K) The theoretical predictions of electric fields under the vertical electric current launching.

(C, F, I, and L) The quantitative comparisons between the experimental measurements and theoretical predictions corresponding to different directions of electric current.

and 6L) exhibit the comparisons between the experimental measurements and theoretical predictions corresponding to horizontal ($\varphi = 0°$) (or vertical ($\varphi = 90°$)) direction of heat flux. It could be seen from the normalized temperature presented in Figures 6C, 6F, 6I, and 6L that the experimental results are in good agreement with the theoretical results under different directions of heat flux, despite whether the air core is wrapped by the camouflage device or not, thus demonstrating the feasibility of the composite structure of matrix.

Similar to Figure 6, the experimental normalized electric distributions with different directions of electric current are presented in Figure 7. Figures 7A and 7D reflect the experimental normalized electric profiles of these two experimental samples illustrated in Figures 4A and 4B, respectively, under the horizontal electric current launching ($\varphi = 0°$). For the vertical electric current launching ($\varphi = 90°$), Figures 7G and 7J reflect the experimental-normalized electric profiles of the same models described earlier. The experimental results of electric camouflage effects for the elliptical air core are as perfect as the thermal camouflage effects. Simultaneously, the numerical simulations combining the theoretically derived material parameters are also carried out to demonstrate the feasibility of the proposed experimental electric camouflage effects. Similar to the thermal simulation results, the electric simulation results are illustrated in Figures 7B, 7E, 7H, and 7K, which are in good agreement with the corresponding experimental results. The comparisons between the experimental measurements and theoretical predictions of normalized electric potential are further proceeded, and the comparison results illustrated in Figures 7C, 7F, 7I, and 7L are consistent with those in Figure 6, thus quantitatively validating the reliability of the experimental electric camouflage results with composite structure from another perspective.

Based on the described experiment and simulation analyses, we obtain that whether the directions of heat flux and electric current are horizontal or vertical, the confocal elliptical camouflage device embedded in the composite structure of matrix could achieve the camouflage effects of the elliptical air core perfectly without disturbing the temperature and electric potential fields, thus realizing the design of the omnidirectional camouflage device with anisotropic confocal elliptic geometry in thermal-electric field successfully.

Conclusions

The key to the design of an omnidirectional camouflage device with anisotropic confocal elliptic geometry lies in the realization of anisotropic matrix material. Owing to the anisotropy of confocal elliptic geometry, the anisotropic thermal and electrical conductivities of matrix material are derived under the vertical and horizontal heat flux and electric current launching. The numerical simulations combining the derived anisotropic material parameters are also carried out to realize the perfect performances of omnidirectional camouflage effect in thermal and electric fields. We further design a composite structure to realize the anisotropic matrix for the experimental implementation. The experiment results indicate that the disturbances of isothermal lines and equipotential lines in the composite structure of matrix of the reference model are eliminated under the work of camouflage device with different directions of heat flux and electric current, thus achieving the omnidirectional thermal-electric camouflage effect experimentally. The comparisons between the experimental measurements and theoretical predictions are further completed to validate the reliability of the experimental results. Our results and the fabrication technique will broaden the research scopes for multiple physical fields, such as electromagnetic waves, acoustics, elastic mechanics, etc., and may pave a way to manipulate these physical fields omnidirectionally and create new functional devices.

Limitations of the study

In this study, we proposed the omnidirectional thermal-electric camouflage device with anisotropic confocal elliptic geometry and used the air and 6061 aluminum to construct the experimental samples. It would be more interesting and valuable to expand the range of materials for the experimental implementation to overcome the limitations of the resistance along the interface of different materials.

STAR★METHODS

Detailed methods are provided in the online version of this paper and include the following:

SUPPLEMENTAL INFORMATION

Supplemental information can be found online at https://doi.org/10.1016/j.isci.2022.104183.

AUTHOR CONTRIBUTIONS

H.F. conceived the idea and performed the theoretical derivations and simulations. H.F. designed the experiments. X.Z. and Y.Z. carried out the experiments. H.F. performed the characterizations. L.Z. contributed to the discussion. H.F. wrote the manuscript and Y.N. revised the manuscript.

DECLARATION OF INTERESTS

The authors declare no competing interests.

REFERENCES

Asrafali, B., Venkateswaran, C., and Yogesh, N. (2021). Spatially squeezed electromagnetic modes of a transformational optics based cavity resonator for targeted material heating. Prog. Electromagn. Res. *106*, 205–214.

Berry, E.A., and Rumpf, R.C. (2020). Generating spatially-variant metamaterial lattices designed from spatial transforms. Prog. Electromagn. Res. *92*, 103–113.

Brun, M., Guenneau, S., and Movchan, A.B. (2009). Achieving control of in-plane elastic waves. Appl. Phys. Lett. *94*, 061903.

Chen, H.Y., and Chan, C.T. (2007). Transformation media that rotate electromagnetic fields. Appl. Phys. Lett. *90*, 241105.

Fakheri, M.H., Abdolali, A., Moradinia, Z., Oraizi, H., and Keivaan, A. (2020). Bi-functional antenna coating for cloaking and directivity enhancement made of isotropic materials. Prog. Electromagn. Res. *90*, 9–18.

Fan, C.Z., Gao, Y., and Huang, J.P. (2008). Shaped graded materials with an apparent negative thermal conductivity. Appl. Phys. Lett. *92*, 251907.

Farhat, M., Guenneau, S., and Enoch, S. (2009). Ultrabroadband elastic cloaking in thin plates. Phys. Rev. Lett. *103*, 024301.

Feng, H.L., and Ni, Y.S. (2022a). Bifunctions of invisible sensors and cloaks in thermal-electric fields. J. Appl. Phys. *131*, 025107.

Feng, H.L., and Ni, Y.S. (2022b). Temperature-dependent switchable thermal bifunctions in different diamond-shaped devices. Appl. Math. Comput. *423*, 127006.

Guenneau, S., Amra, C., and Veynante, D. (2012). Transformation thermodynamics: cloaking and concentrating heat flux. Opt. Express *20*, 8207–8218.

Han, T.C., Bai, X., Gao, D.L., Thong, J.T., Li, B.W., and Qiu, C.W. (2014a). Experimental demonstration of a bilayer thermal cloak. Phys. Rev. Lett. *112*, 054302.

Han, T.C., Yang, P., Li, Y., Lei, D.Y., Li, B.W., Hippalgaonkar, K., and Qiu, C.W. (2018). Full-parameter omnidirectional thermal metadevices of anisotropic geometry. Adv. Mater. *30*, 1804019.

Han, T.C., Ye, H.P., Luo, Y., Yeo, S.P., Teng, J.H., Zhang, S., and Qiu, C.W. (2014b). Manipulating DC currents with bilayer bulk natural materials. Adv. Mater. *26*, 3478–3483.

Han, Z.H., and Zhang, Y.L. (2020). Parameter design of invisible anti-cloak based on nonlinear transformation. Prog. Electromagn. Res. *95*, 63–70.

He, X., and Wu, L.Z. (2013). Thermal transparency with the concept of neutral inclusion. Phys. Rev. E *88*, 033201.

Jiang, W.X., Luo, C.Y., Ma, H.F., Mei, Z.L., and Cui, T.J. (2012). Enhancement of current density by dc electric concentrator. Sci. Rep. *2*, 956.

Lei, M., Wang, J., Dai, G.L., Tan, P., and Huang, J.P. (2021). Temperature-dependent transformation multiphysics and

ambient-adaptive multiphysical metamaterials. EPL *135*, 54003.

Li, J.X., Li, Y., Cao, P.C., Qi, M.H., Zheng, X., Peng, Y.G., Li, B.W., Zhu, X.F., Alù, A., Chen, H.S., and Qiu, C.W. (2022). Reciprocity of thermal diffusion in time-modulated systems. Nat. Commun. *13*, 167.

Li, J.X., Li, Y., Cao, P.C., Yang, T.Z., Zhu, X.F., Wang, W.Y., and Qiu, C.W. (2020). A continuously tunable solid-like convective thermal metadevice on the reciprocal line. Adv. Mater. *32*, 2003823.

Li, J.X., Li, Y., Li, T.L., Wang, W.Y., Li, L.Q., and Qiu, C.W. (2019). Doublet thermal metadevice. Phys. Rev. Appl. *11*, 044021.

Li, J.Y., Gao, Y., and Huang, J.P. (2010). A bifunctional cloak using transformation media. J. Appl. Phys. *108*, 074504.

Li, Y., Bai, X., Yang, T.Z., Luo, H.L., and Qiu, C.W. (2018). Structured thermal surface for radiative camouflage. Nat. Commun. *9*, 273.

Li, Y., Li, W., Han, T.C., Zheng, X., Li, J.X., Li, B.W., Fan, S.H., and Qiu, C.W. (2021). Transforming heat transfer with thermal metamaterials and devices. Nat. Rev. Mater. *6*, 488–507.

Li, Y., Shen, X.Y., Wu, Z.H., Huang, J.Y., Chen, Y.X., Ni, Y.S., and Huang, J.P. (2015). Temperature-dependent transformation thermotics: from switchable thermal cloaks to macroscopic thermal diodes. Phys. Rev. Lett. *115*, 195503.

Ma, Y.G., Liu, Y.C., Raza, M., Wang, Y.D., and He, S.L. (2014). Experimental demonstration of a multiphysics cloak: manipulating heat flux and electric current simultaneously. Phys. Rev. Lett. *113*, 205501.

Milton, G.W. (2004). The Theory of Composites (Cambridge University Press).

Narayana, S., and Sato, Y. (2012). Heat flux manipulation with engineered thermal materials. Phys. Rev. Lett. *108*, 214303.

Narayana, S., Savo, S., and Sato, Y. (2013). Transient heat flux shielding using thermal metamaterials. Appl. Phys. Lett. *102*, 201904.

Pendry, J.B., Schurig, D., and Smith, D.R. (2006). Controlling electromagnetic fields. Science *312*, 1780–1782.

Popa, B.I., Zigoneanu, L., and Cummer, S.A. (2011). Experimental acoustic ground cloak in air. Phys. Rev. Lett. *106*, 253901.

Qu, T., Wang, J., and Huang, J.P. (2021). Manipulating thermoelectric fields with bilayer schemes beyond Laplacian metamaterials. EPL *135*, 54004.

Rahm, M., Schurig, D., Roberts, D.A., Cummer, S.A., Smith, D.R., and Pendry, J.B. (2008). Design of electromagnetic cloaks and concentrators using form-invariant coordinate transformations of Maxwell's equations. Photon. Nanostruct. *6*, 87–95.

Schurig, D., Mock, J.J., Justice, B.J., Cummer, S.A., Pendry, J.B., Starr, A.F., and Smith, D.R. (2006). Metamaterial electromagnetic cloak at microwave frequencies. Science *314*, 977–980.

Xu, G.Q., Dong, K.C., Li, Y., Li, H.G., Liu, K.P., Li, L.Q., Wu, J.Q., and Qiu, C.W. (2020a). Tunable analog thermal material. Nat. Commun. *11*, 6028.

Xu, G.Q., Zhou, X., Zhang, H.C., and Tan, H.-P. (2019). Creating illusion of discrete source array by simultaneously allocating thermal and DC

fields with homogeneous media. Energy Conv. Manag. *187*, 546–553.

Xu, L.J., Huang, J.P., Jiang, T., Zhang, L., and Huang, J.P. (2020b). Thermally invisible sensors. EPL *132*, 14002.

Yang, F., Mei, Z.L., Jin, T.Y., and Cui, T.J. (2012). dc electric invisibility cloak. Phys. Rev. Lett. *109*, 053902.

Yang, S., Wang, J., Dai, G.L., Yang, F.B., and Huang, J.P. (2021). Controlling macroscopic heat transfer with thermal metamaterials: theory, experiment and application. Phys. Rep.-Rev. Sec. Phys. Lett. *908*, 1–65.

Yang, S., Xu, L.J., Wang, R.Z., and Huang, J.P. (2017). Full control of heat transfer in single-particle structural materials. Appl. Phys. Lett. *111*, 121908.

Yang, T.Z., Bai, X., Gao, D.L., Wu, L.Z., Li, B.W., Thong, J.T.L., and Qiu, C.W. (2015). Invisible sensors: simultaneous sensing and camouflaging in multiphysical fields. Adv. Mater. *27*, 7752–7758.

Zhang, S., Xia, C.G., and Fang, N. (2011). Broadband Acoustic cloak for ultrasound waves. Phys. Rev. Lett. *106*, 024301.

Zhang, X.W., He, X., and Wu, L.Z. (2020). Ellipsoidal bifunctional thermal-electric transparent device. Compos. Struct. *234*, 111717.

Zhang, X.W., He, X., and Wu, L.Z. (2021). A bilayer thermal-electric camouflage device suitable for a wide range of natural materials. Compos. Struct. *261*, 113319.

Zhou, X.M., and Hu, G.K. (2006). Design for electromagnetic wave transparency with metamaterials. Phys. Rev. E *74*, 026607.

STAR★METHODS

KEY RESOURCES TABLE

REAGENT or RESOURCE	SOURCE	IDENTIFIER
Software and algorithms		
Matlab R2019a	Mathworks	www.mathworks.com
Adobe illustrator	CC2018	www.adobe.com
Adobe photoshop	CC2018	www.adobe.com

RESOURCE AVAILABILITY

Lead contact

Further information and requests for resources should be directed to and will be fulfilled by the lead contact, Yushan Ni (niyushan@fudan.edu.cn).

Materials availability

This study did not generate new unique reagents.

Data and code availability

- All data reported in this paper will be shared by the lead contact upon request.

- This paper does not report original code.

- Any additional information required to reanalyze the data reported in this paper is available from the lead contact upon request.

EXPERIMENTAL MODEL AND SUBJECT DETAILS

Our study does not use experimental models typical in the life sciences.

METHOD DETAILS

Anisotropic effective parameters of confocal elliptical core-shell structure

Considering the condition that the effective thermal and electric conductivities of confocal elliptical core-shell structure will be changed as the heat flux or electric current flows along different axes, we first derive the anisotropic effective thermal and electric conductivities based on the neutral inclusion method.

It could be seen from Figure S1 that regions I, II and III represent the core, shell, and matrix, respectively. We also use κ_i and σ_i (i = 1, 2, 3) to represent the thermal conductivities and electrical conductivities of the regions described above. The semi-axes of the core and shell are denoted as lc_i and ls_i (i = 1, 2), respectively. Considering the confocal elliptical core-shell structure presented in a uniform thermal (or electric potential) gradient field along the x direction without heat (or electric) source, the temperature and electric potential profiles in different regions can be expressed as below (Milton, 2004)

$$\begin{cases} T_1 = A_1 x \\ T_i = A_i x + B_i x \int_{\rho_c}^{\rho} \dfrac{d\rho}{(\rho + lc_1^2) g(\rho)} \end{cases} \qquad \text{(Equation 1)}$$

$$\begin{cases} \varphi_1 = C_1 x \\ \varphi_i = C_i x + D_i x \int_{\rho_c}^{\rho} \dfrac{d\rho}{(\rho + lc_1^2) g(\rho)} \end{cases} \qquad \text{(Equation 2)}$$

where T_1 (or φ_1) represents the temperature (or electric potential) of the core. T_i (or φ_i) (i = 2,3) represent the temperature (or electric potential) of the shell and matrix, respectively.

Then, we use the mathematical methods (Xu et al., 2020b) to proceed the partial derivatives and integrations in Equations 1 and 2.

$$\frac{\partial x}{\partial \rho} = \frac{x}{2(\rho + lc_1^2)} \qquad \text{(Equation 3)}$$

$$\int_{\rho_c}^{\rho_s} \frac{d\rho}{(\rho + lc_1^2)g(\rho)} = \int_{\rho_c}^{\infty} \frac{d\rho}{(\rho + lc_1^2)g(\rho)} - \int_{\rho_s}^{\infty} \frac{d\rho}{(\rho + lc_1^2)g(\rho)} = \frac{2}{g(\rho_c)}Lc_1 - \frac{2}{g(\rho_s)}Ls_1 \qquad \text{(Equation 4)}$$

where $g(\rho_c)$ and $g(\rho_s)$ are the area parameters of the core and shell, respectively. Among which, $g(\rho_c) = \sqrt{(lc_1^2 + \rho_c)(lc_2^2 + \rho_c)} = lc_1\ lc_2$ and $g(\rho_s) = \sqrt{(lc_1^2 + \rho_s)(lc_2^2 + \rho_s)} = ls_1\ ls_2$. $\rho_c\ (\rho_c = 0)$ denotes the confocal elliptical core surface with semi-axis lc_i (i = 1, 2). ρ_s presents the confocal elliptical shell surface with semi-axis ls_i (i = 1, 2). Lc_1 and Ls_1 are the depolarizing factors along x axis of the core and shell, respectively. For confocal ellipse, $Lc_1 = \frac{lc_2}{lc_1 + lc_2}$ and $Ls_1 = \frac{ls_2}{ls_1 + ls_2}$.

The associated boundary conditions combining the Equations 1, 2, 3 and 4 are as follows.

1. The thermal and electric fields in the matrix are uniformly distributed:

$$\begin{cases} B_3 = 0 \\ D_3 = 0 \end{cases} \qquad \text{(Equation 5)}$$

2. The temperature and electric potential are continuous along the elliptical core surface (ρ_c) and shell surface (ρ_s):

$$\begin{cases} A_1 = A_2 \\ C_1 = C_2 \\ A_3 = A_2 + 2B_2\left(\frac{Lc_1}{lc_1 lc_2} - \frac{Ls_1}{ls_1 ls_2}\right) \\ C_3 = C_2 + 2D_2\left(\frac{Lc_1}{lc_1 lc_2} - \frac{Ls_1}{ls_1 ls_2}\right) \end{cases} \qquad \text{(Equation 6)}$$

3. The heat flux and electric current are also continuous along the elliptical core surface (ρ_c) and shell surface (ρ_s):

$$\begin{cases} \kappa_1 A_1 = \kappa_2\left(A_2 + \frac{2B_2}{lc_1 lc_2}\right) \\ \sigma_1 C_1 = \sigma_2\left(C_2 + \frac{2D_2}{lc_1 lc_2}\right) \\ \kappa_3 A_3 = \kappa_2\left[A_2 + \frac{2B_2}{ls_1 ls_2} + 2B_2\left(\frac{Lc_1}{lc_1 lc_2} - \frac{Ls_1}{ls_1 ls_2}\right)\right] \\ \sigma_3 C_3 = \sigma_2\left[C_2 + \frac{2D_2}{ls_1 ls_2} + 2D_2\left(\frac{Lc_1}{lc_1 lc_2} - \frac{Ls_1}{ls_1 ls_2}\right)\right] \end{cases} \qquad \text{(Equation 7)}$$

Meanwhile, the relationship between the semi-axes of the core and shell could be obtained due to the confocal properties of the elliptical core-shell structure.

$$(lc_1)^2 - (lc_2)^2 = (ls_1)^2 - (ls_2)^2 \qquad \text{(Equation 8)}$$

Based on the above discussions, the effective thermal and electric conductivities of confocal elliptical core-shell structure under the horizontal direction (x direction) of heat flux and electric current could be obtained by solving Equations 5, 6, 7 and 8.

$$\begin{cases} \kappa_{eff\ x} = \kappa_2 + \dfrac{\kappa_2(\kappa_1 - \kappa_2)P_1}{\kappa_2 + (\kappa_1 - \kappa_2)(Lc_1 - P_1\ Ls_1)} \\ \sigma_{eff\ x} = \sigma_2 + \dfrac{\sigma_2(\sigma_1 - \sigma_2)P_1}{\sigma_2 + (\sigma_1 - \sigma_2)(Lc_1 - P_1\ Ls_1)} \end{cases} \qquad \text{(Equation 9)}$$

where κ_1 and κ_2 are the thermal conductivities of the core and shell. σ_1 and σ_2 are the electric conductivities of the core and shell. P_1 is the area fraction of the core for the shell, and $P_1 = \frac{lc_1}{ls_1} \frac{lc_2}{ls_2}$.

Due to the geometric anisotropy of confocal ellipse, the effective thermal and electric conductivities of confocal elliptical core-shell structure will be changed when the heat flux and electric current flow along the y direction. Similar to the derivation of x-directional parameters, the effective thermal and electrical conductivities under vertical heat and electric launching could be obtained below.

$$\begin{cases} \kappa_{eff\ y} = \kappa_2 + \dfrac{\kappa_2(\kappa_1 - \kappa_2)P_1}{\kappa_2 + (\kappa_1 - \kappa_2)\left(Lc_2 - P_1\ Ls_2\right)} \\[4mm] \sigma_{eff\ y} = \sigma_2 + \dfrac{\sigma_2(\sigma_1 - \sigma_2)P_1}{\sigma_2 + (\sigma_1 - \sigma_2)\left(Lc_2 - P_1\ Ls_2\right)} \end{cases} \qquad \text{(Equation 10)}$$

where Lc_2 and Ls_2 are the depolarizing factors along y axis of the core and shell, respectively. For confocal ellipse, $Lc_2 = \frac{lc_1}{lc_1 + lc_2}$ and $Ls_2 = \frac{ls_1}{ls_1 + ls_2}$.

To sum up, the anisotropic effective thermal and electrical conductivities of the confocal elliptical core-shell structure could be obtained by solving Equations 9 and 10 simultaneously.

A composite structure with natural materials

The specific process of constructing the composite structure consists of two steps, as shown in Figure S2. Firstly, the anisotropic matrix illustrated in Figure S2A is transformed into alternating-multilayered structure illustrated in Figure S2B based on the effective medium theory (Guenneau et al., 2012), and the alternating-multilayered structure possesses isotropic material parameters for each layer. However, the isotropic material parameters of each layer are arbitrary, not natural materials. Then, as for each layer of material, we use the single-particle structure method (Yang et al., 2017) to design particle structure composed of natural materials to satisfy the arbitrary thermal and electric conductivities, simultaneously. The thermal and electric conductivities of the particle structure can be obtained as follows.

$$\begin{cases} \kappa_{i\ th} = \kappa_\beta + \dfrac{2\kappa_\beta\left(\kappa_\alpha - \kappa_\beta\right)f_1}{2\kappa_\beta + \left(\kappa_\alpha - \kappa_\beta\right)\left(1 - f_1\right)} \\[4mm] \sigma_{i\ th} = \sigma_\beta + \dfrac{2\sigma_\beta(\sigma_\alpha - \sigma_\beta)f_1}{2\sigma_\beta + (\sigma_\alpha - \sigma_\beta)\left(1 - f_1\right)} \end{cases} \qquad \text{(Equation 11)}$$

$$\begin{cases} \kappa_{j\ th} = \kappa_\eta + \dfrac{2\kappa_\eta(\kappa_\varepsilon - \kappa_\eta)f_2}{2\kappa_\eta + (\kappa_\varepsilon - \kappa_\eta)\left(1 - f_2\right)} \\[4mm] \sigma_{j\ th} = \sigma_\eta + \dfrac{2\sigma_\eta(\sigma_\varepsilon - \sigma_\eta)f_2}{2\sigma_\eta + (\sigma_\varepsilon - \sigma_\eta)\left(1 - f_2\right)} \end{cases} \qquad \text{(Equation 12)}$$

where $\kappa_{i\ th}$, $\kappa_{j\ th}$ and σ_{ith}, σ_{jth} ($i = 1, 3, 5 \ldots$) ($j = 2, 4, 6 \ldots$) are the arbitrary thermal and electric conductivities of different layers, respectively. κ_α, κ_β, κ_ε, κ_η and σ_α σ_β, σ_ε, σ_η are the thermal and electric conductivities of natural materials, respectively. f_1 and f_2 are the area fractions of the particle structures, and $f_1 = \frac{\pi r_1^2}{a^2}$, $f_2 = \frac{\pi r_2^2}{a^2}$. r_1 and r_2 are the radii of the circular particles. a is the side length of a square.

When the side length of the square and the natural material parameters satisfying the concept of neutral inclusion are given, the radii of the circular particles could be calculated based on Equations 11 and 12 to realize the arbitrary isotropic material parameters for each layer. Finally, through the array of the particle structures, the construction of anisotropic matrix could be realized illustrated in Figure S2C, which may provide a suggestion to realize anisotropic thermal and electric conductivities using composite structure with natural materials.

Next, we further verify the feasibility of the proposed method. The theoretical anisotropic thermal and electrical conductivities of matrix illustrated in Figure S2A could be calculated based on the Equations 9 and 10. After that, we use the simulation method to calculate the effective thermal and electrical conductivities of the structure presented in Figure S2C. The theoretical and simulation results of anisotropic thermal and electrical conductivities are presented below.

The theoretical and simulation results of anisotropic thermal and electrical conductivities

Anisotropic parameters	Theoretical results (TR)	Simulation results (SR)	(SR-TR)/TR
κ_x W/(m*K)	91.22	94.03	3%
κ_y W/(m*K)	70.75	73.58	4%
σ_x S/m	1.47E7	1.51E7	2.7%
σ_y S/m	1.14E7	1.18E7	3.5%

It can be obtained that the error between theoretical result and simulation result of κ_x or σ_x is controlled at about 3%, and the error between theoretical result and simulation result of κ_y or σ_y is controlled at about 4%, which indicates that the simulation results agree well with the theoretical results, thus verifying the feasibility of the proposed method.

QUANTIFICATION AND STATISTICAL ANALYSIS

Our study does not include quantification or statistical analysis.